

**SYNTHESIS AND CHARACTERIZATION OF  
WO<sub>x</sub>/ZnO NANOCOMPOSITES ON  
POLYETHYLENE TEREPHTHALATE (PET)  
FIBER FOR PHOTOCATALYTIC APPLICATION**

**MYO THUYA THEIN**

**UNIVERSITI SAINS MALAYSIA**

**2016**

**SYNTHESIS AND CHARACTERIZATION OF WO<sub>x</sub>/ZnO  
NANOCOMPOSITES ON POLYETHYLENE TEREPHTHALATE (PET)  
FIBER FOR PHOTOCATALYTIC APPLICATION**

**by**

**MYO THUYA THEIN**

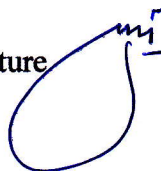
**Thesis submitted in fulfillment of the requirements  
for the degree of Doctor of Philosophy**

**June 2016**

## DECLARATION

I hereby declare that I have conducted, completed the research work and written the thesis entitles "SYNTHESIS AND CHARACTERIZATION OF WO<sub>x</sub>/ZnO NANOCOMPOSITES ON POLYETHYLENE TEREPHTHALATE (PET) FIBER FOR PHOTOCATALYTIC APPLICATION". I also declare that it has not been previously submitted for the award of any degree or diploma or other similar title of this for any other examining body of University.


Name of Student: Myo Thuya Thein

Signature 

Date: 7 June 2016

Witness by

Supervisor: Dr Pung Swee Yong

Signature 

Date: 7 June 2016

DR. PUNG SWEE YONG  
SCHOOL OF MATERIALS AND MINERAL RESOURCES ENGINEERING  
ENGINEERING CAMPUS  
UNIVERSITI SAINS MALYSIA  
14300 NIBONG TEBAL, PULAU PINANG, MALAYSIA.

Co-supervisor: Assoc. Prof. Dr. Zainovia Lockman

Signature 

Date: 7 June 2016

ASSOC. PROF. DR. ZAINOVIA LOCKMAN  
School of Materials & Mineral Resources Engineering  
Engineering Campus  
Universiti Sains Malaysia  
14300 Nibong Tebal  
Seberang Perai Selatan  
Penang  
MALAYSIA

Co-supervisor: Prof. Dr. Mitsuru Itoh

Signature

Date: 7 June 2016

## ACKNOWLEDGEMENTS

I am grateful to School of Materials and Mineral Resources Engineering (SMMRE), University Sains Malaysia (USM) for offering an opportunity for me to study PhD in nanomaterials with sufficient research facilities, great supports from administrative, academic and technical staffs. I also sincerely thank to Japan International Cooperation Agency (JICA) and AUN/SEED-Net under collaborative research program (CR) (304/PBAHAN/6050277/A119) as well as USM Research University Grant (RU) (1001/ PBAHAN/ 814200) for providing the research funding to conduct this study.

I am deeply grateful to my supervisor, Dr. Pung Swee Yong for his supervision and advice on my study. He listened to my ideas and discussed friendly with me which led to the key insights of my work. He is a very good advisor. It was a great opportunity to study my doctoral research under his supervision. Besides, he has been patient and encouraged me when I was facing challenges. I have never forgotten his kindness.

I also would like to express my sincere gratitude to my co-supervisors, Prof. Dr. Azizan Aziz (USM), Prof. Dr. Mitsuru Itoh (Tokyo Institute of Technology, Japan) and Assoc. Prof. Dr. Zainovia Lockman (USM) for their continuous support, patience, motivation, enthusiasm and immense knowledge throughout my doctoral study.

I would like to convey my appreciation to the Dean of SMMRE, Prof. Dr. Zuhailawati Bt. Hussain and former Dean Prof. Dr. Hanafi B. Ismail, for their concern and help during my study. I would also like to deliver my sincere appreciation to the Chair Coordinating Committee of AUN/SEED-Net at SMMRE,

Prof. Dr. Ahmad Fauzi Mohd Noor for his kindness and support to finish my study smoothly.

My special thanks and appreciation are also extended to these people, who helped me to accomplish my research work: Mr. Zulkurnain Bin Hasbolah, Mr. Mohammad Azrul Bin, Mr. Muhammad Khairi Bin, Mr. Mohamad Zaini Bin Saari, Mr. Abdul Rashid Bin Selamat, Mr. Kemuridan Bin Md. Desa, Mdm. Fong Lee Lee and Mdm. Haslina Bt Zulkifli.

Last but not least, I am grateful to my beloved parent and wife for unconditional supports, motivation and encouragement. I also deeply thank to my colleagues in USM for their support and friendships throughout my study.

Thank you to all of you.

## TABLE OF CONTENTS

Acknowledgements .....	ii
Table of Contents .....	iv
List of Tables .....	xi
List of Figures .....	xiii
List of Abbreviations .....	xxvi
List of Symbols .....	xxvii
Abstrak .....	xxviii
Abstract .....	xxx
CHAPTER 1 – INTRODUCTION	
1.1 Research Background .....	1
1.2 Problem Statements .....	5
1.3 Research Objectives .....	7
1.4 Research scope .....	7
CHAPTER 2 – LITERATURE REVIEW	
2.1 Introduction .....	10
2.2 Physical properties of ZnO .....	11
2.2.1 Crystal structure .....	12
2.2.2 Optical property .....	14
2.2.3 Electrical property .....	15
2.2.4 Mechanical property .....	16
2.3 Synthesis of ZnO nanostructures .....	16

2.3.1	Synthesis of ZnO nanostructures using solution routes .....	18
2.3.2	Synthesis of ZnO nanostructure by vapor routes .....	27
2.3.3	Comparison between ZnO nanostructures synthesized by various techniques .....	28
2.4	Nanocomposites .....	31
2.4.1	Au/ZnO nanocomposite .....	31
2.4.2	Ag/ZnO nanocomposites .....	32
2.4.3	Ag <sub>2</sub> O/ZnO nanocomposites .....	33
2.4.4	CuO/ZnO nanocomposites .....	34
2.4.5	Ag <sub>2</sub> S/ZnO nanocomposites .....	35
2.4.6	CdS/ZnO nanocomposites .....	36
2.4.7	In <sub>2</sub> S <sub>3</sub> /ZnO nanocomposites .....	37
2.5	Textile dyeing industry .....	38
2.5.1	Classification of dyes .....	39
2.5.2	Production and discharge of dyes .....	40
2.6	Current technology available for dye treatment .....	40
2.6.1	Physical treatment .....	41
2.6.1.1	Adsorption .....	41
2.6.1.2	Ion exchange .....	41
2.6.1.3	Filtration .....	42
2.6.2	Biological treatment .....	42
2.6.2.1	Aerobic .....	43
2.6.2.2	Anaerobic/aerobic–anaerobic .....	43

2.6.3	Chemical treatment .....	44
2.6.3.1	Coagulation and flocculation.....	44
2.6.3.2	Chemical oxidation .....	45
2.7	Advanced oxidation processes (AOP) .....	46
2.8	Comparison between organic dye removal techniques in wastewater .....	47
2.9	Photocatalytic degradation of organic dyes using semiconductor photocatalysts .....	47
2.9.1	Ultraviolet (UV) light responsive semiconductor photocatalysts .....	51
2.9.2	Visible light responsive semiconductor photocatalysts .....	56
2.9.3	Factors affecting photocatalytic efficiency of semiconductor photocatalysts .....	59
2.9.3.1	Effect of initial dye concentration .....	59
2.9.3.2	Effect of catalyst loading .....	61
2.9.3.3	Effect of irradiation time .....	62
2.9.3.4	Effect of pH .....	64
2.9.3.5	Effect of wavelength and light intensity .....	66
2.9.4	Photodegradation mechanism of organic compound by semiconductor photocatalysts .....	67
2.9.4.1	Isopropanol (i-PrOH) - scavenger of hydroxyl radical ( $\text{OH}^\bullet$ ) .....	70
2.9.4.2	Benzoquinone (BQ) - scavenger of superoxide anion ( $\text{O}_2^{\bullet-}$ ) .....	71
2.9.4.3	Potassium iodide (KI) - scavenger of hole ( $h^+$ ) .....	72



## CHAPTER 3 – MATERIALS AND METHODOLOGY

3.1	Introduction .....	74
3.2	Raw materials and chemicals .....	74
3.3	Experimental procedure .....	77
3.3.1	Synthesis and characterization of ZnO nanostructures .....	78
3.3.1.1	Synthesis and characterization of ZnO rods .....	78
3.3.1.2	Synthesis and characterization of ZnO nanodisks ...	79
3.3.2	Synthesis and characterization of Ni/ZnO nanocomposites ...	81
3.3.3	Synthesis of WO <sub>x</sub> /ZnO and W/ZnO nanocomposites .....	84
3.3.4	Synthesis of ZnO rods on PET fibers .....	87
3.3.5	Synthesis of WO <sub>x</sub> /ZnO nanocomposites grown on PET fibers	89
3.4	Characterization techniques .....	91
3.4.1	X-ray diffraction spectroscopy (XRD) .....	91
3.4.2	Field-emission scanning electron microscopy (FESEM) .....	92
3.4.3	Energy dispersive X-ray spectroscopy (EDX) .....	93
3.4.4	Surface charge .....	94
3.4.5	Transmission electron microscopy (TEM)/ High resolution transmission electron microscopy (HRTEM) .....	94
3.4.6	Ultraviolet-visible spectroscopy (UV-Vis) .....	95
3.4.7	Photoluminescence spectroscopy (PL) .....	96
3.5	Photocatalytic degradation of organic dyes using semiconductor photocatalysts .....	97

## CHAPTER 4 – RESULTS AND DISCUSSION

4.1	Introduction .....	99
4.2	Synthesis and characterization of ZnO nanostructures .....	99
4.2.1	Effect of capping agent .....	99
4.2.1.1	Growth mechanism of stacked ZnO rods and ZnO flowers .....	102
4.2.1.2	Photocatalytic study of ZnO rods and ZnO flowers ..	106
4.2.2	Effect of growth duration .....	109
4.2.2.1	Photocatalytic study of ZnO rods .....	112
4.2.3	Effect of growth temperature .....	117
4.2.3.1	Photocatalytic study of ZnO rods .....	121
4.2.4	Effect of aluminium sulphate and ammonia hydroxide .....	123
4.2.4.1	Growth mechanism of ZnO nanodisks .....	127
4.2.4.2	Photocatalytic study of ZnO nanodisks .....	130
4.2.5	A comparison between ZnO rods and ZnO nanodisks .....	132
4.2.5.1	Photocatalytic study of ZnO rods and ZnO nanodisks .....	139
4.2.5.2	Identification of dominant reactive species in photocatalytic process under UV light irradiation ...	143
4.3	Synthesis and characterization of Ni/ZnO nanocomposites and WO <sub>x</sub> /ZnO nanocomposites .....	148
4.3.1	Effect of calcination temperature on Ni/ZnO nanocomposites	148
4.3.1.1	Photocatalytic study of Ni/ZnO nanocomposites .....	153
4.3.2	Effect of nickel nitrate concentration on Ni/ZnO nanocomposites .....	156

4.3.2.1	Photocatalytic study of Ni/ZnO nanocomposites ....	162
4.3.3	Effect of deposition duration on WO <sub>x</sub> /ZnO nanocomposites ...	167
4.3.3.1	Photocatalytic study of WO <sub>x</sub> /ZnO nanocomposites ..	170
4.3.4	Effect of deposition temperature .....	173
4.3.4.1	Photocatalytic study of WO <sub>x</sub> /ZnO nanocomposites ..	177
4.3.5	Effect of solution concentration .....	179
4.3.5.1	Photocatalytic study of WO <sub>x</sub> /ZnO nanocomposites ..	184
4.3.6	Effect of reduction under hydrogen atmosphere .....	186
4.3.6.1	Photocatalytic study of reduced WO <sub>x</sub> /ZnO nanocomposites .....	188
4.3.7	A comparison between the Ni/ZnO and WO <sub>x</sub> /ZnO nanocomposites .....	190
4.3.7.1	Photocatalytic study of Ni/ZnO and WO <sub>x</sub> /ZnO nanocomposites .....	197
4.3.7.2	Identification of dominant reactive species in photocatalytic process by Ni/ZnO nanocomposites (0.03NZ500R500) under UV light irradiation and its photodegradation mechanism .....	201
4.3.7.3	Identification of dominant reactive species in photocatalytic process by WO <sub>x</sub> /ZnO nanocomposites (0.04WZ) under UV light irradiation and its photodegradation mechanism .....	203
4.3.7.4	The photocatalytic performance of 0.04WZ sample in removal of different organic dye .....	206

4.4	Synthesis and characterization of ZnO rods grown on PET fibers .....	209
4.4.1	Effect of growth duration .....	210
4.4.1.1	Photocatalytic study of ZnO rods grown on PET fibers .....	213
4.4.2	Effect of growth temperature .....	216
4.4.2.1	Photocatalytic study of ZnO rods grown on PET fibers .....	218
4.4.3	Effect of solution concentration .....	220
4.4.3.1	Photocatalytic study of ZnO rods grown on PET fibers .....	224
4.5	Synthesis and characterization of WO <sub>x</sub> /ZnO nanocomposites grown on PET fibers .....	227
4.5.1	Effect of solution concentration .....	227
4.5.1.1	Photocatalytic study of WO <sub>x</sub> /ZnO nanocomposites grown on PET fibers .....	230
 CHAPTER 5 – CONCLUSION AND FUTURE WORK		
5.1	Conclusion .....	236
5.2	Future work .....	240
	References .....	242
	Appendices	
	List of Publications	

## LIST OF TABLES

		Page
Table 2.1	Effect of growth temperature on the morphology of ZnO nanostructures synthesized by solution precipitation method (Sepulveda-Guzman et al., 2009)	19
Table 2.2	Effect of growth duration on the morphology of ZnO nanostructures synthesized by solution precipitation method (Yang et al., 2008)	20
Table 2.3	Effect of zinc nitrate concentration on the morphology of ZnO nanostructures synthesized by solution precipitation method (Yang et al., 2008)	21
Table 2.4	Effect of growth temperature on the morphology of ZnO nanostructures by hydrothermal (Li et al., 2008)	22
Table 2.5	Effect of growth duration on the morphology of ZnO nanostructures by hydrothermal (Zhang et al., 2002)	23
Table 2.6	Effect of solution concentration on the morphology of ZnO nanostructures by hydrothermal (Polsongkram et al., 2008)	24
Table 2.7	Effect of growth temperature on the morphology of ZnO particles by sol-gel method (Khan et al., 2014)	25
Table 2.8	Effect of growth duration on the morphology of ZnO particles by sol-gel method (Pung et al., 2012)	26
Table 2.9	Effect of $Zn_{ace}/O_{xa}$ molar ratio on the morphology of ZnO particles by sol-gel method (Ba-Abbad et al., 2013)	26
Table 2.10	Advantages and disadvantages of solution routes	29
Table 2.11	Advantages and disadvantages of vapor routes	30
Table 2.12	Global export and import market of different dyes (Ghaly et al., 2014)	40
Table 2.13	Comparative degradation efficiency of different advanced oxidation processes (AOP)	48
Table 2.14	Advantages and factors to be considered for treating textile wastewater	49

Table 2.15	Comparison of photocatalytic performance of ZnO based nanocomposites in removal of organic dyes under UV light	55
Table 2.16	Effect of initial dye concentration on the rate of degradation of acid brown 14 (Sakthivel et al., 2003)	60
Table 2.17	Effect of catalyst loading on degradation rate of acid brown 14 (Sakthivel et al., 2003)	62
Table 2.18	Photodegradation efficiency of acid brown 14 vs. irradiation time (Sakthivel et al., 2003)	63
Table 2.19	Effect of pH on degradation rate of acid brown 14 (Sakthivel et al., 2003)	65
Table 2.20	Effect of light intensity on the degradation of acid brown 14 (Sakthivel et al., 2003)	67
Table 2.21	Photoinduced active species and their corresponded scavengers	69
Table 3.1	Raw materials and chemicals used in synthesizing of ZnO nanostructure, Ni/ZnO and WO <sub>x</sub> /ZnO nanocomposites, ZnO rods and WO <sub>x</sub> /ZnO nanocomposites grown on the PET fibers via solution precipitation method	75
Table 3.2	Synthesis parameters for ZnO rods prepared via solution precipitation method	78
Table 3.3	Synthesis parameters for ZnO nanodisks using solution precipitation method	80
Table 3.4	Synthesis parameters for Ni/ZnO nanocomposites via solution precipitation method	82
Table 3.5	Synthesis parameters for WO <sub>x</sub> /ZnO and W/ZnO nanocomposites via solution precipitation method	85
Table 3.6	Synthesis parameters for ZnO rods grown on PET fiber via solution precipitation method	88
Table 3.7	Synthesis parameters for WO <sub>x</sub> /ZnO nanocomposites grown on PET fiber via solution precipitation method	90
Table 4.1	Comparison of ZnO rods and ZnO nanodisks	143
Table 5.1	Comparison between ZnO nanostructures and ZnO based nanocomposites under UV and visible light irradiation	240

## LIST OF FIGURES

		Page
Figure 1.1	The number of clean and polluted rivers in Malaysia from year 2005 to 2013 (Department of Environment, 2013)	2
Figure 1.2	Contribution of scheduled waste from textile industry at different states in Malaysia. (Pang and Abdullah, 2013)	3
Figure 1.3	Flow chart of research work	9
Figure 2.1	The relationship between specific surface area ( $\text{sq.m kg}^{-1}$ ) of a spherical particle and its size (diameter in nm) (density of $1000 \text{ kg m}^{-3}$ ). Specific surface area increases as particles become smaller (Navarro et al., 2008)	11
Figure 2.2	Stick and ball representation unit cell of ZnO crystal structures: (a) cubic rocksalt (B1), (b) cubic zinc blende (B3), and (c) hexagonal wurtzite (B4). The shaded gray and black spheres denote Zn and O atoms, respectively (Özgür et al., 2005)	12
Figure 2.3	Schematic representation of a wurtzite structure of ZnO. The grey and yellow spheres denote Zn and O atoms, respectively (Özgür et al., 2005)	13
Figure 2.4	Zn-terminated (0001) and O-terminated ( $000\bar{1}$ ) surface of hexagonal wurtzite (a) ZnO rod-like structure (Pauporté, 2009) and (b) ZnO disk-like structure (Zhang et al., 2008)	13
Figure 2.5	Room temperature photoluminescence spectrum of ZnO nanowires excited at 325 nm (Liu et al., 2012)	15
Figure 2.6	ZnO nanostructure with different morphologies: (a) Sphere (Koplin et al., 2006) (b) nanowires (Greene et al., 2006) (c) rods (Zhang et al., 2014) (d) nanoflowers (Krishnan and Pradeep, 2009) (e) nanorings (Jung et al., 2009) and (f) nanodisks (Abbas et al., 2013)	18
Figure 2.7	SEM images of (a) ZnO rods electrodeposited on ITO glass and Au/ZnO nanocomposites as-prepared at galvanic replacement reaction of (b) 200 s, (c) 400 s and (d) 600 s (Myung et al., 2013)	32
Figure 2.8	SEM images of (a) ZnO microrods and (b) Ag coated ZnO microrods (Lu et al., 2008)	33
Figure 2.9	SEM images of (a) ZnO nanorods and (b) $\text{Ag}_2\text{O}/\text{ZnO}$ nanorods (Lin et al., 2009)	34

Figure 2.10	SEM images of (a) ZnO nanorods grown on glass and CuO/ZnO nanocomposites prepared at different UV light irradiation of (b) 30 min, (c) 60 min and (d) 90 min (Ang et al., 2013)	35
Figure 2.11	FESEM images of (a) ZnO nanorods and (b) Ag <sub>2</sub> S/ZnO nanocomposites (Khanchandani et al., 2014)	36
Figure 2.12	FESEM images of (a) ZnO nanorods and (b) CdS/ZnO nanocomposites (Khanchandani et al., 2012)	37
Figure 2.13	FESEM images of (a) ZnO nanorods and (b) In <sub>2</sub> S <sub>3</sub> /ZnO nanocomposites (Khanchandani et al., 2013)	38
Figure 2.14	Molecular structure of Indigo (Vuorema, 2008)	38
Figure 2.15	Molecular structure of rhodamine B (RhB) (Zhuang et al., 2010)	39
Figure 2.16	Electronic structure of different metal oxides and the relative position of their band edges vs. some key redox potentials (Ghicov and Schmuki, 2009)	51
Figure 2.17	(a) SEM image of ZnO nanorods and (b) their photocatalytic activity using MO solution under UV light irradiation at constant time interval (Tang, 2013)	52
Figure 2.18	(a) SEM image of ZnO nanowires and (b) their photocatalytic activity in photodegradation of RhB solution under UV light irradiation (Zeng et al., 2009)	53
Figure 2.19	FESEM images of (a) ZnO nanorods, (b) CuO/ZnO (1:99), (c) CuO/ZnO (3:97), (d) CuO/ZnO (5:95) (e) CuO/ZnO (10:90) and (f) CuO/ZnO (50:50) nanocomposites (Saravanan et al., 2013)	57
Figure 2.20	Photodegradation of (a) MB and (b) MO at different exposure times under visible light illumination (Saravanan et al., 2013)	57
Figure 2.21	(a) FESEM image and (b) Adsorption spectra of MB aqueous solution degraded by V <sub>2</sub> O <sub>5</sub> /ZnO nanocomposite (Saravanan et al., 2014)	58
Figure 2.22	Effect of initial concentration of Acid brown 14 on the degradation efficiency by (a) ZnO and (b) TiO <sub>2</sub> . Catalyst amount = 2.5 g l <sup>-1</sup> ; pH = 9.41–9.98 (Sakthivel et al., 2003)	60



Figure 2.23	Effect of catalyst loading on the degradation of Acid brown 14 using (a) ZnO and (b) TiO <sub>2</sub> . Acid brown 14 = $5 \times 10^{-4} \text{ mol l}^{-1}$ ; pH = 9.93 (Sakthivel et al., 2003)	61
Figure 2.24	Formation of inorganic ions with different irradiated time in acid brown 14 (Sakthivel et al., 2003)	63
Figure 2.25	Influence of pH on the adsorption and rate of degradation of acid brown 14. Acid brown 14 = $5 \times 10^{-4} \text{ mol l}^{-1}$ ; Catalyst amount = $2.5 \text{ g l}^{-1}$ (Sakthivel et al., 2003)	64
Figure 2.26	Schematic representation of the processes taking place at the catalyst surface (Helen, 2014)	68
Figure 2.27	(a) Effect of <i>i</i> -PrOH on degradation rates of CBZ in aqueous TiO <sub>2</sub> and ZnO suspensions, CBZ = 10mg/l; TiO <sub>2</sub> = ZnO = 100mg/l. (b) Effect of <i>i</i> -PrOH on degradation rates of IBP in aqueous TiO <sub>2</sub> and ZnO suspensions, IBP = 10mg/l; TiO <sub>2</sub> = ZnO = 100mg/l (Georgaki et al., 2014)	71
Figure 2.28	0.18Pt-TiO <sub>2</sub> photocatalyzed degradation of 2,4,6-TCP in the presence of scavengers (Hu et al., 2012)	72
Figure 2.29	Effect of the iodine addition to the reaction system at two different concentrations: $7.65 \times 10^{-4}$ (O) and $7.65 \times 10^{-3}$ (Δ) compared to the photocatalysed degradation of the antibiotic ( $7.65 \times 10^{-5} \text{ mol l}^{-1}$ ) (■) (Palominos et al., 2008)	73
Figure 3.1	Flow chart represents the synthesis and characterization of ZnO rods via solution precipitation method for photocatalytic study	79
Figure 3.2	Flow chart represents the synthesis and characterization of ZnO nanodisks via solution precipitation method for photocatalytic study	81
Figure 3.3	Flow chart of synthesis and characterization of Ni/ZnO nanocomposites via solution precipitation method for photocatalytic study	83
Figure 3.4	Heating profile of the calcination process for the formation of NiO/ZnO nanocomposites	84
Figure 3.5	Heating profile of the reduction process under hydrogen atmosphere for the formation of Ni/ZnO nanocomposites	84
Figure 3.6	Flow chart of synthesis and characterization of WO <sub>x</sub> /ZnO and W/ZnO nanocomposites using solution precipitation method for photocatalytic study	86

Figure 3.7	Heating profile of the reduction process under hydrogen atmosphere for the formation of W/ZnO nanocomposites	87
Figure 3.8	Flow charts of (a) deposition of ZnO seed layers and (b) synthesis and characterization of ZnO rods grown on PET fibers using solution precipitation method for photocatalytic study	89
Figure 3.9	Flow chart of synthesis and characterization of WO <sub>x</sub> /ZnO nanocomposites grown on PET fiber via solution precipitation method for photocatalytic study	90
Figure 3.10	Schematic of photodegradation of RhB under circulation condition	98
Figure 4.1	XRD patterns of ZnO particles synthesized without and with PVP	101
Figure 4.2	FESEM images of ZnO rods synthesized (a) without and (b) with PVP	101
Figure 4.3	Schematic representation of cross sectional view of ZnO rod	103
Figure 4.4	Zeta potential of ZnO rods	104
Figure 4.5	Schematic representation of growth mechanism of ZnO flower	105
Figure 4.6	Schematic representation of growth mechanism of stacked ZnO rods using solution precipitation technique	106
Figure 4.7	UV-Vis absorbance spectra of RhB solution degraded by (a) without ZnO catalysts, (b) ZnO flowers (synthesized without PVP) and (c) ZnO rods (synthesized with PVP) under UV irradiation	108
Figure 4.8	(a) Photodegradation efficiencies, (b) pseudo first-order kinetic reaction with respect to UV light irradiation and (c) rate constant of ZnO rods synthesized without and with PVP in degrading RhB solution under UV irradiation	108
Figure 4.9	XRD patterns of ZnO particles synthesized at different growth durations	110
Figure 4.10	FESEM images of ZnO rods at growth duration of (a) 15 min, (b) 30 min, (c) 180 min, (d) 300 min, (e) 420 min and (f) 600 min	111

Figure 4.11	(a) Average lengths, diameters and (b) aspect ratios of ZnO rods synthesized at various growth durations	112
Figure 4.12	UV-Vis adsorption spectra of RhB solution degraded by ZnO rods synthesized at growth duration of (a) 15 min, (b) 30 min, (c) 180 min, (d) 300 min, and (e) 420 min, and (f) 600 min under UV irradiation	114
Figure 4.13	(a) Photodegradation efficiencies, (b) pseudo first-order kinetic reaction with respect to the UV light irradiation time and (c) rate constant of ZnO rods synthesized at different growth duration under UV irradiation	115
Figure 4.14	Effect of exposure surface area of ZnO rods on photodegradation of RhB solution under UV irradiation	115
Figure 4.15	Photodegradation of RhB dye by ZnO particles	116
Figure 4.16	XRD patterns of ZnO particles at different growth temperature	118
Figure 4.17	FESEM images of ZnO rods synthesized at growth temperature of (a) 70 °C, (b) 90 °C and 98 °C	119
Figure 4.18	(a) Average lengths, diameters and (b) aspect ratios of ZnO rods synthesized at different growth temperature	120
Figure 4.19	EDX spectrum of ZnO rods synthesized at growth temperature of 90 °C	120
Figure 4.20	UV-Vis absorbance spectra of RhB solution degraded by ZnO rods synthesized at growth temperature of (a) 70 °C, (b) 90 °C and (c) 98 °C under UV irradiation	121
Figure 4.21	(a) Photodegradation efficiencies, (b) pseudo first-order kinetic reaction with respect to the UV light irradiation and (c) rate constant of ZnO rods synthesized at different growth temperature	122
Figure 4.22	XRD patterns of ZnO particles synthesized using different amount of ammonia hydroxide	124
Figure 4.23	The weight fraction of ZnO particles synthesized using different amount of ammonia hydroxide	125
Figure 4.24	FESEM images of ZnO hexagonal nanodisks synthesized using (a) 1.0 ml, (b) 1.5 ml, (c) 2.0 ml, (d) 2.5 ml, and (e) 3.0 ml of NH <sub>4</sub> OH and (f) diameters of ZnO hexagonal nanodisks using different amount of NH <sub>4</sub> OH	126

Figure 4.25	The EDX spectrum of ZnO hexagonal nanodisks synthesized using 2.0 ml of NH <sub>4</sub> OH	127
Figure 4.26	Schematic representation of growth mechanism of ZnO hexagonal nanodisks	129
Figure 4.27	Zeta potential of ZnO nanodisks	129
Figure 4.28	UV-Vis adsorption spectra of RhB solution degraded by ZnO nanodisk synthesized at (a) 1.0 ml, (b) 1.5 ml, (c) 2.0 ml, (d) 2.5 ml and (e) 3.0 ml of NH <sub>4</sub> OH	131
Figure 4.29	(a) Degradation efficiencies, (b) pseudo first-order kinetic reaction with respect to the UV light irradiation and (c) rate constant of ZnO nanodisks synthesized at different volume of NH <sub>4</sub> OH	132
Figure 4.30	XRD patterns of ZnO rods and ZnO nanodisks	133
Figure 4.31	TEM images of (a) ZnO rods and (b) ZnO nanodisks	134
Figure 4.32	HRTEM images of (a) ZnO rod and (b) ZnO nanodisk	134
Figure 4.33	SAED patterns of (a) ZnO rod and (b) ZnO nanodisk	135
Figure 4.34	EDX mapping of ZnO rod: (a) Zn element and (b) O element	135
Figure 4.35	(a) TEM image and EDX mapping of ZnO nanodisk: (b) Zn element (c) O element and (d) Al element	136
Figure 4.36	UV-Vis adsorption spectra of (a) ZnO rods and (b) ZnO nanodisks	137
Figure 4.37	(a) Room temperature PL spectra (b) UV emission of ZnO nanodisks and (c) $R_{(UV/vis)}$ of ZnO nanostructures	138
Figure 4.38	(a) Photodegradation efficiencies, (b) pseudo first-order kinetic reactions with respect to UV light irradiation and (c) rate constants of ZnO rods and ZnO nanodisks	140
Figure 4.39	UV-Vis adsorption spectra of RhB solution photodegraded by (a) ZnO rods and (b) ZnO nanodisks under visible light irradiation	141
Figure 4.40	(a) Photodegradation efficiencies, (b) pseudo first-order kinetic reaction with respect to the visible light irradiation time and (c) rate constants of ZnO rods and ZnO nanodisks	142

Figure 4.41	Scavengers tests on the photodegradation efficiency of ZnO rods in degrading RhB solution under UV irradiation	144
Figure 4.42	The band position of semiconductor photocatalyst in NHE diagram (Lam et al., 2015, Xie et al., 2014)	146
Figure 4.43	Schematic of photodegradation mechanism of RhB dye by ZnO rods	147
Figure 4.44	XRD patterns of Ni/ZnO nanocomposites synthesized at different calcination temperature	150
Figure 4.45	FESEM images of Ni/ZnO nanocomposites calcinated at (a) 250 °C, (b) 350 °C, (c) 500 °C, (d) 600 °C and (f) 700 °C	152
Figure 4.46	(a) Average lengths, diameters and (b) aspect ratios of Ni/ZnO nanocomposites with respect to the calcination temperature	152
Figure 4.47	EDX spectrum of Ni/ZnO nanocomposites synthesized at calcination temperature of 500 °C	152
Figure 4.48	UV-Vis adsorption spectra of RhB solution degraded by (a) without catalysts and with Ni/ZnO nanocomposites synthesized at calcination temperature of (b) 250 °C, (c) 350 °C, (d) 500 °C, (e) 600 °C and (f) 700 °C	154
Figure 4.49	(a) Photodegradation efficiencies, (b) pseudo first-order kinetic reaction with respect to the UV light irradiation time and (c) rate constants of Ni/ZnO nanocomposites synthesized at different calcination temperature	155
Figure 4.50	XRD patterns of Ni/ZnO nanocomposites synthesized at different nickel nitrate concentration	157
Figure 4.51	FESEM images of (a) ZnO rods and Ni/ZnO nanocomposites synthesized at nickel nitrate concentration of (b) 0.02 M, (c) 0.03 M, (d) 0.07 M and (e) 0.14 M	158
Figure 4.52	(a) Average lengths, diameters and (b) aspect ratios of Ni/ZnO nanocomposites with respect to the solution concentration	158
Figure 4.53	(a) EDX spectrum of 0.03NZ500R500 sample and (b) Ni atomic percentage of Ni/ZnO nanocomposites synthesized using various concentration of nickel nitrate solution	159

Figure 4.54	(a) Room temperature PL spectra (b) room temperature PL spectra in visible region and (c) ratios of UV to visible light intensity of Ni/ZnO nanocomposites synthesized at different nickel nitrate concentration	160
Figure 4.55	Effect of surface plasmon resonance on the enhancement of UV emission and suppression of visible light emission of Ni/ZnO nanocomposites	161
Figure 4.56	UV-Vis adsorption spectra of RhB solution degraded under UV irradiation by (a) without catalyst, (b) ZnO rods and Ni/ZnO nanocomposites synthesized using concentration of nickel nitrate (c) 0.02 M, (d) 0.03 M, (e) 0.07 M and (f) 0.14 M	163
Figure 4.57	(a) Photodegradation efficiencies, (b) pseudo first-order kinetic reaction with respect to the UV light irradiation and (c) rate constant of RhB, ZnO rods and Ni/ZnO nanocomposites synthesized at different nickel nitrate concentration	164
Figure 4.58	Hypsochromic shift of maximum adsorption peak of photo-degraded RhB solution by 0.03NZ500R500 sample	165
Figure 4.59	Correlation plot of photodegradation efficiency/rate constant of RhB solution by Ni/ZnO nanocomposites as a function of $R_{UV/Vis}$ of PL analysis	166
Figure 4.60	XRD patterns of $WO_x/ZnO$ nanocomposites synthesized at different deposition duration	168
Figure 4.61	FESEM images of (a) ZnO rods and $WO_x/ZnO$ nanocomposites synthesized at deposition duration of (b) 1 h, (c) 3 h, (d) 6 h, (e) 12 h and (f) 24 h	169
Figure 4.62	(a) Average lengths, diameters and (b) aspect ratios of $WO_x/ZnO$ nanocomposites with respect to the deposition duration	170
Figure 4.63	(a) EDX spectrum of 0.01WZ1 sample and (b) tungsten atomic percentage of $WO_x/ZnO$ nanocomposites synthesized at different deposition duration	170
Figure 4.64	UV-Vis adsorption spectra of RhB solution photodegraded by (a) ZnO and $WO_x/ZnO$ nanocomposites synthesized at deposition duration of (b) 1 h, (c) 3 h, (d) 6 h, (e) 12 h and (f) 24 h	172

Figure 4.65	(a) Photodegradation efficiencies, (b) pseudo first-order kinetic reaction with respect to the UV light irradiation and (c) rate constant of WO <sub>x</sub> /ZnO nanocomposites synthesized at different deposition duration	173
Figure 4.66	XRD patterns of WO <sub>x</sub> /ZnO nanocomposites synthesized at different deposition temperature	175
Figure 4.67	FESEM images of (a) ZnO rods and WO <sub>x</sub> /ZnO nanocomposites prepared at (b) 25 °C, (c) 50 °C, (d) 70 °C and (e) 90 °C	176
Figure 4.68	(a) Average lengths, diameters and (b) aspect ratios of WO <sub>x</sub> /ZnO nanocomposites with respect to the deposition temperature	176
Figure 4.69	(a) EDX spectrum of 0.01WZ25 sample and (b) tungsten atomic percentage of WO <sub>x</sub> /ZnO nanocomposites synthesized at different deposition temperature	176
Figure 4.70	UV-Vis adsorption spectra of RhB dye solution photodegraded by (a) ZnO rods and WO <sub>x</sub> /ZnO nanocomposites synthesized at deposition temperature of (b) 25 °C, (c) 50 °C, (d) 70 °C and (e) 90 °C	178
Figure 4.71	(a) Photodegradation efficiencies, (b) pseudo first-order kinetic reaction with respect to the UV light irradiation and (c) rate constant of WO <sub>x</sub> /ZnO nanocomposites synthesized at different deposition temperature	179
Figure 4.72	XRD patterns of WO <sub>x</sub> /ZnO nanocomposites synthesized at different solution concentration	180
Figure 4.73	FESEM images of (a) ZnO rods and WO <sub>x</sub> /ZnO nanocomposites synthesized at sodium tungstate solution concentration of (b) 0.01 M, (c) 0.02 M, (d) 0.04 M, (e) 0.06 M and (f) 0.09 M	182
Figure 4.74	(a) Average lengths, diameters and (b) aspect ratios of WO <sub>x</sub> /ZnO nanocomposites with respect to the solution concentration	182
Figure 4.75	(a) EDX spectrum of 0.04WZ sample and (b) tungsten atomic percentage of WO <sub>x</sub> /ZnO nanocomposites synthesized at different solution concentration	182
Figure 4.76	(a) Room temperature PL spectra and (b) the value of $R_{UV/Vis}$ of WO <sub>x</sub> /ZnO nanocomposites synthesized at different sodium tungstate solution	183

Figure 4.77	UV-Vis adsorption spectra of RhB dye solution photodegraded by (a) ZnO (b) 0.01WZ, (c) 0.02WZ, (d) 0.04WZ, (e) 0.06WZ and (f) 0.09WZ samples	185
Figure 4.78	(a) Degradation efficiencies, (b) pseudo first-order kinetic reaction with respect to the UV light irradiation and (c) rate constant of $WO_x/ZnO$ nanocomposites synthesized at different solution concentration	186
Figure 4.79	XRD pattern of before and after hydrogen reduced 0.04WZR500 sample	187
Figure 4.80	FESEM image of hydrogen reduced 0.04WZR500 sample	188
Figure 4.81	EDX spectrum of 0.04WZR500 sample	188
Figure 4.82	(a) UV-Vis adsorption spectra, (b) degradation efficiency of RhB solution degraded by reduced $WO_x/ZnO$ nanocomposites and (c) pseudo first-order kinetic reaction with respect to the UV light irradiation time	189
Figure 4.83	XPS spectra of 0.03NZ500R500 sample (a) wide scan, (b) Zn 2p core-level spectra, (c) O 1s core-level spectra and (d) Ni 2p core-level spectra	191
Figure 4.84	XPS spectra of 0.04WZ sample (a) wide scan, (b) Zn 2p core-level spectra, (c) O 1s core-level spectra and (d) W 4f core-level spectra	192
Figure 4.85	TEM images of (a) 0.03NZ500R500 and (b) 0.04WZ samples	193
Figure 4.86	HRTEM images of (a) 0.03NZ500R500 and (b) 0.04WZ samples	193
Figure 4.87	EDX elemental mapping of (a) Zn, (b) O and (c) Ni element of 0.03NZ500R500 sample	194
Figure 4.88	(a) TEM images of 0.04WZ sample and its EDX mapping of (b) Zn, (c) O and (d) W element	195
Figure 4.89	Light adsorption spectra of (a) Ni/ZnO nanocomposites, (b) $WO_x/ZnO$ nanocomposites and their corresponded band gap energy for (c) Ni/ZnO nanocomposites and (d) $WO_x/ZnO$ nanocomposites	196
Figure 4.90	RTPL spectra of ZnO, 0.03NZ500R500 and 0.04WZ samples	197